Received: 25 March 2022 | Revised: 29 July 2022 | Accepted: 5 August 2022

DOI: 10.1111/ppl.13762

ECOPHYSIOLOGY, STRESS AND ADAPTATION

Physiologia Plantarum

Challenging the water stress index concept: Thermographic assessment of *Arabidopsis* transpiration

Andreas M. Savvides[1] | Aaron I. Velez-Ramirez[2,3] | Vasileios Fotopoulos[1]

[1]Department of Agricultural Sciences, Biotechnology and Food Science, Cyprus University of Technology, Limassol, Cyprus

[2]Laboratorio de Ciencias Agrogenómicas, Escuela Nacional de Estudios Superiores Unidad León, Universidad Nacional Autónoma de México, León, Mexico

[3]Laboratorio Nacional PlanTECC, Escuela Nacional de Estudios Superiores Unidad León, Universidad Nacional Autónoma de México, León, Mexico

Correspondence
Andreas M. Savvides and Vasileios Fotopoulos, Department of Agricultural Sciences, Biotechnology and Food Science, Cyprus University of Technology, Limassol, Cyprus.
Email: andreas.m.savvides@gmail.com and vassilis.fotopoulos@cut.ac.cy

Edited by K.-J. Dietz

Abstract

Water stress may greatly limit plant functionality and growth. Stomatal closure and consequently reduced transpiration are considered as early and sensitive plant responses to drought and salinity stress. An important consequence of stomatal closure under water stress is the rise of leaf temperature (T_{leaf}), yet T_{leaf} is not only fluctuating with stomatal closure. It is regulated by several plant parameters and environmental factors. Thermal imaging and different stress indices, incorporating actual leaf/crop temperature and reference temperatures, were developed in previous studies toward normalizing for effects unassociated to water stress on T_{leaf}, aiming at a more efficient water stress assessment. The concept of stress indices has not been extensively studied on the model plant *Arabidopsis thaliana*. Therefore, the aim of this study was to examine the different indices employed in previous studies in assessing rosette transpiration rate (E) in *Arabidopsis* plants grown under two different light environments and subjected to salinity. After salinity imposition, E was gravimetrically quantified, and thermal imaging was employed to quantify rosette ($T_{rosette}$) and artificial reference temperature (T_{wet}, T_{dry}). $T_{rosette}$ and several water stress indices were tested for their relation to E. Among the microclimatic growth conditions tested, $RWSI_1$ ($[T_{rosette} - T_{wet}]/[T_{dry} - T_{wet}]$) and $RWSI_2$ ($[T_{dry} - T_{rosette}]/[T_{dry} - T_{wet}]$) were well linearly-related to E, irrespective of the light environment, while the sole use of either T_{wet} or T_{dry} in different combinations with $T_{rosette}$ returned less accurate results. This study provides evidence that selected combinations of $T_{rosette}$, T_{dry}, and T_{wet} can be utilized to assess E under water stress irrespective of the light environment.

1 | INTRODUCTION

As sessile organisms, plants are exposed to several adverse environmental conditions during their life span and respond accordingly through a variety of mechanisms to survive and reproduce. Drought and salinity are major factors limiting plant functionality and growth (Daryanto et al., 2017; González Guzmán et al., 2022; Zörb et al., 2019) and their impacts on plants are exacerbating due to climate change (Corwin, 2021; Mukherjee et al., 2018). The early responses to drought and salinity have been considered largely identical (Flexas et al., 2004; Munns, 2002). To minimize water loss to the atmosphere (i.e., transpiration) under limited water uptake and maintain their internal water status, seed plants rapidly close their stomata (Lawson & Vialet-Chabrand, 2019; McAdam & Brodribb, 2012). Stomatal closure and, consequently, the reduced transpiration rates are considered as (1) early and sensitive responses of plants (Munns, 2002) and (2) tolerance traits to water deficit (Bartlett et al., 2016). Although stomatal conductance and transpiration rates are widely and precisely quantified at leaf level using portable gas exchange photosynthesis systems (e.g., Savvides et al., 2012; Savvides & Fotopoulos, 2018), leaf porometers (Filippou et al., 2011, 2021), and gravimetric techniques (Cirelli et al., 2012), faster and

higher throughput quantification methods are needed to accelerate the production of new knowledge in the field.

An important consequence of stomatal closure under water stress is the reduction in heat dissipation through transpiration (i.e., latent heat transfer) and, therefore, the rise of leaf temperature (Jones, 1999a). Plant temperatures can be monitored using a variety of methodologies depending on the aim of the study and the available tools (e.g., Savvides et al., 2013, 2016). Infrared thermography is a technique using a thermal imager to detect infrared radiation (i.e., heat) emitted from an object and processing it to estimate the object's temperature. Infrared thermography (Jones, 2004) is one of the most widely used imaging techniques in the field of plant–environment interactions (Costa et al., 2013; Maes & Steppe, 2012). According to Jones (1999a), the idea of using leaf (T_{leaf}) or canopy temperature (T_{canopy}) as an indicator of plant water stress was proposed over half a century ago (e.g., Tanner, 1963). Considering the leaf energy balance equation, T_{leaf} is not only varying with stomatal closure, but it is also regulated by several plant parameters and environmental factors (Jones, 1992, 2004) such as air temperature (T_{air}), radiation, air vapor pressure deficit (VPD), and wind speed (Costa et al., 2013). Therefore, if a study aims, for example, to compare the physiological responses of a plant to different water stress levels under stable weather conditions, T_{leaf} alone can be utilized as a reliable stress indicator. On the other hand, if the weather conditions are fluctuating during the study, then their effects on T_{leaf} should be normalized to properly assess the plant stress level (Jones et al., 2009).

Several stress indices have been developed through the years to normalize for weather conditions (reviewed in Costa et al., 2013). Initially, the development of the "stress degree day" (i.e., the accumulated difference in temperature between the leaf or crop canopy and the air along a certain period; Jackson et al., 1977) represents an improvement over the use of T_{canopy} alone, since it allows for fluctuating T_{air} (Costa et al., 2013). Thereafter, it was suggested that $T_{canopy} - T_{air}$ depends on VPD (Jackson et al., 1981). Under non-limiting soil water conditions, a crop transpires at a potential rate; however, the latter increases with increasing VPD (Costa et al., 2013). The linear relationship between $T_{canopy} - T_{air}$ and VPD was called "the theoretical non-water stress baseline" (Jackson et al., 1981). At a given VPD, for a selected crop, this baseline provides the minimum value to $T_{canopy} - T_{air}$. $T_{canopy} - T_{air}$ of a non-transpiring crop is insensitive to VPD, provides the upper limit to $T_{canopy} - T_{air}$, and can be estimated if wind speed and net solar radiation are known (Costa et al., 2013). Jackson et al. (1981) developed a crop water stress index (CWSI) based on $T_{canopy} - T_{air}$, the lower (i.e., the minimum possible value) and the upper limit (i.e., the maximum possible value) to $T_{canopy} - T_{air}$. The higher the CWSI, the higher the estimated crop stress level (Costa et al., 2013). Determining the theoretical non-water stress baseline is time-consuming and CWSI does not account for changes in aerodynamic resistance and radiation (Costa et al., 2013; Prashar & Jones, 2016). Jones (1999a) proposed the replacement of the theoretical non-water stress baseline and the upper limit with the temperatures of two objects imaged in the same environment and at the same time with the canopy of interest. The two objects represent a canopy (or a leaf) with maximum transpiration and a non-transpiring surface. This version of CWSI and a rearrangement of the latter (I_G; proportional to stomatal conductance; Jones, 1999a; Maes & Steppe, 2012) yielded better results across a range of weather conditions (Jones, 1999a). However, CWSI and I_G, estimated based on reference surfaces, depend on the boundary layer conductance (i.e., the ease in which gas and energy are exchanged through the boundary layer, a thin zone of calm air surrounding a leaf), which in turn depends on the air flow near the leaf surface (Jones, 1999a; Jones, 2002; Maes & Steppe, 2012). Therefore, variations in wind speed and/or crop or leaf traits shaping boundary layer conductance should be considered when utilizing the water stress index concept (Jones, 2004; Maes & Steppe, 2012). In addition, more candidate indices, using one of the reference surfaces, were tested across a range of conditions in previous studies (e.g., Poirier-Pocovi & Bailey, 2020).

Water stress indices are commonly related to stomatal conductance, a measure of stomatal closure (Jones, 2002), usually quantified by porometric techniques (Jones, 1999a; Jones, 2002; Poirier-Pocovi & Bailey, 2020). However, these leaf-level measurements may not be representative of the whole-plant responses and water loss (Cirelli et al., 2012). Some of the possible reasons for this are: (1) the spatial heterogeneity in stomatal behavior present at leaf- and plant-scale (McAusland et al., 2015); (2) the plant architecture and the heterogeneous air flow influencing boundary layer conductance (Rice et al., 2001); and (3) the vapor pressure difference between the canopy and the atmosphere (i.e., the driving force for transpiration), which can differ in a closed system such as a porometer. On the other hand, whole-plant transpiration (E) measurement is of interest in the context of whole-plant physiology (Cirelli et al., 2012). E is the water loss in the form of water vapor from a plant surface, and thus a determining parameter of plant water use efficiency and crop stress tolerance (Ryan et al., 2016). E is not only governed by stomatal conductance but also by the boundary layer conductance and leaf-to-air vapor pressure difference, and thus the environmental factors and plant traits determining the three distinct parameters (Jones, 1992). Therefore, E estimation based on thermal imaging is essential to integrate sub-organismal mechanisms, such as stomatal closure at leaf level, and the environment into an easy-to-measure whole-plant level response and water loss.

Arabidopsis thaliana (L.) is a model plant (Meyerowitz, 2001) highly employed in high-throughput phenotyping platforms (Jangra et al., 2021) to advance our understanding of genotype-to-phenotype transitions. Thermal imaging has been employed and various stress indices tested against different physiological parameters across a range of conditions and plant species in the form of proximal or remote sensing (reviewed in Pineda et al., 2021). Despite the wide application of thermal imaging in *A. thaliana* research (e.g., Klem et al., 2016; Merlot et al., 2002; Orzechowska et al., 2020), the concept of water stress indices has not been extensively tested. The main aim of this study was to examine the use of different water stress

indices employed in previous studies (Costa et al., 2013; Jones, 1999a; Poirier-Pocovi & Bailey, 2020) in assessing rosette transpiration rate in *A. thaliana*. For that purpose, we used plants grown under two different light environments and subjected to different salinity levels.

2 | MATERIALS AND METHODS

2.1 | Plant material and growth conditions

Seeds of *A. thaliana* (L.) Heynh. ecotype Columbia (Col-0) were stratified (i.e., subjected for 3 days at 4°C) and germinated in soil (Plantaflor® potting soil, DE). Following plant emergence, 3 days after stratification (3 DAS), young seedlings were transplanted in custom-made pots (Figure 1B) and subjected to two different photosynthetic photon flux densities (PPFD), 80 and 168 μmol m^{-2} s^{-1} provided by fluorescent tubes (54 W/T5/840 FHO, Sylvania Lighting). Exactly 40 plants per PPFD level were grown on growth stands in a climate room. Growth under two PPFD levels but in a single climate room with controlled air temperature, humidity, and air flow promoted the reduction of local gradients in environmental factors other than radiation. During growth, the mean air temperature (T_{air}) was approximately 22°C, and the mean relative humidity (RH) was approximately 55% (TT4 Humidity monitor, Sensitech). No considerable differences were observed between the two different PPFDs regarding T_{air} and RH.

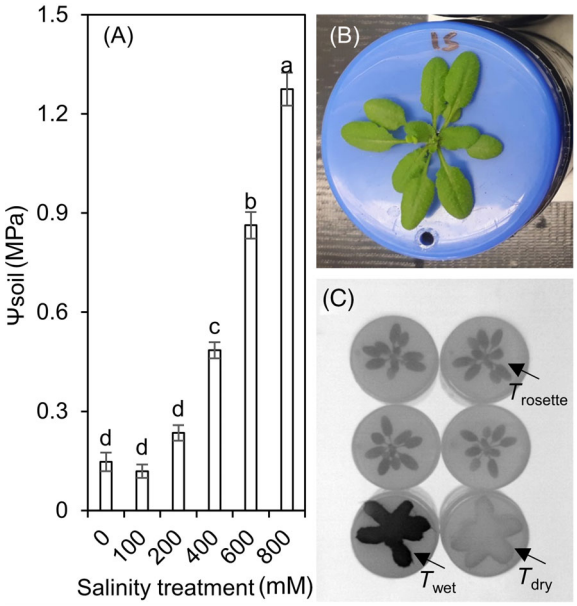

FIGURE 1 (A) Soil water potential (Ψ_{soil}) quantified for each salinity treatment. Different letters above the bars indicate significant differences between the means ($p < 0.05$; $n = 5$ measurements, each on an independent plant) by one-way analysis of variance (Tukey test). Error bars indicate the standard error of the mean (SEM). (B) Custom-made plant containers used in the study. (C) Sample infrared image indicating the rosette temperature ($T_{rosette}$), reference wet (T_{wet}), and dry (T_{dry}) temperatures.

2.2 | Salinity treatments

Twenty-four days after stratification (24 DAS), each plant was irrigated with 50 ml NaCl solution. Six concentrations of NaCl were used (0, 100, 200, 400, 600, and 800 mM). Five plants per light treatment and salinity level were used. Salinity stress was maintained for 4 days until the end of the experiment. Soil water potential (Ψ_{soil}) for every container was measured in soil samples using a dewpoint water potential meter (WP4, Decagon Devices, Inc.) immediately after the end of the experiment (Figure 1A). As 800 mM NaCl concentration caused severe stress resulting in significant leaf area loss within the first day after stress induction, plants treated with 800 mM NaCl were not included in further analysis.

2.3 | Transpiration rate, projected rosette area, and final growth

Plant water loss was quantified according to Wituszyńska et al. (2013) and Wituszynska and Karpiński (2014), with some adjustments. Transparent cylindrical plastic containers (270 ml volume) were filled with potting soil (Plantaflor® potting soil, DE) and sealed with blue caps (Figure 1B). Caps (38.5 cm^2 surface area) were used to minimize soil evaporation. The cap's blue color contrasted with the rosette and facilitated image segmentation. Two holes (0.1 cm^2 surface area) were drilled, one at the center and one at the rear of each cap to assist the outgrowth of the plants and irrigation, respectively. Water loss through the holes due to evaporation was quantified during the experiment in containers without plants and was subtracted from the overall water loss. The transparent part of the container was covered prior to the experiment with black tape to avoid light penetration into the soil and roots (Cabrera et al., 2022). During growth and salinity treatments, diel water loss was quantified by measuring the container weight using a balance (0.001 g resolution) before and after irrigation. Plants were irrigated when necessary to maintain the initial container weight and soil moisture. Projected rosette area (PRA) was quantified throughout the experiment and used as an indicator of plant growth in time as well as for the calculation of rosette transpiration rate (*E*, water loss per rosette area per unit time). PRA was quantified using red, green, and blue (RGB) imaging and image analysis using the freeware ImageJ (Schneider et al., 2012) as described by Savvides and Fotopoulos (2018). At the end of the experiment, rosettes were dissected and final fresh (FW) and dry weights (DW, after drying in an oven at 80°C) were quantified. Rosette water content (WC) was then estimated based on the following formula ([FW − DW]/DW) × 100.

2.4 | Thermography

All thermal images were obtained with a thermal camera Optris PI450 (Optris GmbH), equipped with a 38° × 29° lens (focal length, $f = 15$ mm) that operates in the wavebands 7.5–13 μm and has thermal sensitivity of 0.04 K and optical resolution of 382 × 288 pixels.

Rosette emissivity was set at 0.95 (Jones, 2004). The thermal and RGB camera were secured on a stand with the lenses vertically positioned (using a clinometer). The two cameras were positioned 20 cm above the surface of the plants and between the light sources (i.e., to avoid plant shading). Images were captured during the morning (2 h after the lights were turned on) of the second and fourth day after stress imposition. Four plants were imaged simultaneously in a single acquisition with two reference objects (Figure 1C) under their growth conditions (i.e., low light [LL] or high light [HL]). The reference objects were dry and wet pieces of green felt (Jones, 1999b; Vialet-Chabrand & Lawson, 2020) placed on two identical plastic containers representing a non-transpiring surface and a surface with infinite conductance, respectively. The wet reference was rewetted when needed to maintain it saturated. The plants and reference objects were moved in place (i.e., under the growth light intensity) for imaging and the images were captured 15 min after relocation to ensure object temperature stabilization.

Thermal images were segmented (i.e., background removed) using masks obtained from processing RGB images. This was necessary because rosette and pot caps had a similar temperature in some treatments, making it difficult to segment using simple threshold algorithms. A commercial software was used for most of the procedure (i.e., Vision Development Module version 18.5 for LabVIEW from NI). First, original RGB images (Figure S1A) were transformed to the International Commission on Illumination (CIE) L*a*b* color space using the "IMAQ RGBToColor 2 VI" procedure. Each of the three CIE L*a*b* channels was stored and processed independently; Figure S1B–D shows each channel. Then, pot caps were found in the thermal (Figure S2A) and CIE b* channel images (Figure S1D) by looking for circular edges using the "IMAQ Find Circular Edge 3 VI" algorithm. This allowed us to find coordinates for caps centers in each pot for both images (Figures S1E and S2B). As the used lenses were not telecentric and each camera had a slightly different angle with respect to the rosettes plane, there were small perspective differences between the thermal and RGB/CIE L*a*b* images. To correct for this, we used in Python the "getPerspectiveTransform()" algorithm from the OpenCV library (Bradski, 2000). As the pots were ordered in a rectangular array in each image, we used the pot centers from four pots located at the corners of each image as reference coordinates for the quadrangle vertices (Figures S1E and S2B). The resulting images had the same apparent perspective (Figures S1F–H and S2C) as if the thermal and RGB/CIE L*a*b* images were acquired by placing both cameras in spatial superposition. Next, we obtained a segmentation mask for the coin (added to each image as size reference) using the CIE L* channel and the "IMAQ Find Circular Edge 3 VI" algorithm. Coin segmentation mask is shown in Figure S1I.

To segment the rosettes, we used the CIE a* and b* channels. First, the "IMAQ AutoMThreshold 2 VI" classified the pixels into six classes according to their intensity in both the a* and b* channels, independently. Then, the "IMAQ MultiThreshold VI" selected the classes that corresponded to the rosettes; in this step, a human curator aided in selecting the right classes. Next, the results from processing the CIE a* and b* channels were added together, and a segmentation mask was obtained using the "IMAQ AutoBThreshold" algorithm. In the rosette segmentation mask, the coin was removed by using the coin segmentation mask previously obtained from the CIE L* channel. Finally, border and small particles were removed from the rosette segmentation mask using the "IMAQ RejectBorder VI" and "IMAQ RemoveParticle VI" algorithms, respectively; for the latter algorithm, 10 erosions were used. Figure S1J shows the resulting rosette segmentation mask. Rosette segmentation mask was then downscaled to a tenth of its original size using the zero-order option from the "IMAQ Resample VI" procedure; this was done to account for the lower resolution in the thermal images. Next, borders in the scaled rosette segmentation mask were identified by the "IMAQ EdgeDetection VI" algorithm, using the differentiation method. This allowed us to precisely identify the border (i.e., edges) between leaves and the cap background. Figure S1K,L shows the identified edges, and Figure S1I shows a single rosette edge superimposed on the CIA a* to show the resulting high-quality match. The same procedure failed to find edges in the thermal images; therefore, a different procedure was used to approximate the edges' locations.

Edges between leaves and background in the thermal images were approximated using the following procedure. First, thermal images were smoothed using linear filtering by the "IMAQ Convolute VI" algorithm; for this, a 3×3 Gaussian convolution matrix (i.e., kernel) was used. Next, the "IMAQ CannyEdgeDetection VI" algorithm was used to find edges. Although this procedure was not perfect (Figure S2D), it detected enough edges between leaves and background to use the latter as guidelines to align this image with the CIE L*a*b*-derived rosette segmentation edge mask.

Alignment between both edge masks was done by changing scale, rotation, and *XY* position of the rosette edge mask (Figure S1K), and then subtracting from it the thermal image edge mask (Figure S2D). If the edges of both images are aligned, an image subtraction deletes the edges; if the sum of all pixel values in the subtraction result is low, it means that the alignment is good (Figure S2E,F). Therefore, we minimized the mask subtraction result to find the best alignment. This was one by nesting for loops, which tested 29,000 alignment options for each image. We used the "IMAQ Rotate VI", "IMAQ Shift VI", and "IMAQ Resample VI" algorithms for rotating, displacing in *X* and *Y* direction, and scaling the edge masks, respectively. Rotation and scaling were done using bipolar interpolation. Figure S2E shows a CIE L*a*b* rosette mask not yet perfectly aligned, scaled, and rotated on top of an IR edge mask. After testing thousands of alignments, the algorithm finds the rotation, scaling, and displacement needed for a perfect match (Figure S2F). A human curator inspected the best alignment (Figure S2G) for approval. Figure S2H shows an example of the resulting IR segmentation mask.

2.5 | Stress indices

In this study, the terms "canopy" and/or "leaf temperatures" used in literature were replaced by "rosette temperature" and, correspondingly, CWSI was renamed as RWSI.

$T_{rosette}$, $T_{rosette} - T_{wet}$, $T_{dry} - T_{rosette}$, and five stress indices based on $T_{rosette}$, T_{dry}, and T_{wet} developed/tested in previous literature (Jones, 1999a; Poirier-Pocovi & Bailey, 2020) were evaluated as to their relationship with E.

$T_{dry} - T_{rosette}$ is the difference between the temperature of a non-transpiring surface and the temperature of a rosette. $T_{dry} - T_{rosette}$ is expected to have values higher than zero and decrease with decreasing stomatal conductance under a stable aerial environment.

$T_{rosette} - T_{wet}$ is the difference between a rosette and a wet surface's temperature. $T_{rosette} - T_{wet}$ is expected to have values higher than zero and increases with decreasing stomatal conductance under a stable aerial environment.

CWSI using artificial references (referred to as I_2 in the study by Jones, 1999a) is an index analogous to a previously developed index derived from energy balance equations (Idso et al., 1981; Jackson et al., 1981):

$$CWSI = 1 - \frac{\lambda E}{\lambda E_{pot}} = \frac{(T_{canopy} - T_{air}) - (T_{canopy} - T_{air})_{nwsb}}{(T_{canopy} - T_{air})_{ul} - (T_{canopy} - T_{air})_{nwsb}} \quad (1)$$

An analytical explanation and steps toward the derived equation (Equation 1) are given by Jackson et al. (1981) and Maes and Steppe (2012). λ is the latent heat of vaporization of water. The potential crop is identical to the actual crop but it is transpiring at maximal rate (E_{pot}). The ratio between actual and potential transpiration (E/E_{pot}) ranges from one to zero when the actual crop does not transpire. $T_{canopy} - T_{air}$ is the measured difference, $(T_{canopy} - T_{air})_{nwsb}$ is the estimated difference at the same VPD under non-limiting soil water conditions (non-water-stressed baseline), and $(T_{canopy} - T_{air})_{ul}$ is the non-transpiring upper limit (Costa et al., 2013). CWSI is expected to have values between zero and one and increase with increasing water deficit. CWSI does not account for changes in T_{canopy} due to radiation and aerodynamic resistance, and the non-water-stressed baseline can be different under different radiation conditions (Costa et al., 2013; Jones, 1999b) and the non-transpiring upper limit may also vary (Ben-Gal et al., 2009).

Jones (1999a) substituted the temperature of a non-transpiring canopy with T_{dry} (i.e., the temperature of a dry surface) and base temperature, the temperature of a non-stressed canopy, with T_{wet} (i.e., the temperature of a wet surface):

$$RWSI_1 = \frac{T_{rosette} - T_{wet}}{T_{dry} - T_{wet}} \quad (2)$$

Even though, there is no theoretical relation between $RWSI_1$ and $1 - [\lambda E/\lambda E_{pot}]$, this approach is more practical because the temperatures of (artificial) reference surfaces are measured directly with $T_{rosette}$ and no additional microclimatic measurements are required (Maes & Steppe, 2012). $RWSI_1$ is expected to have values closer to zero; the larger the difference between T_{dry} and $T_{rosette}$ and the closer to one, the smaller is the difference between T_{dry} and $T_{rosette}$.

Thermal index of relative stomatal conductance (I_G; Equation 3) is an alternative index based on the rearrangement of the energy balance equation (referred to as I_4 in the study by Jones, 1999a). For most values of g_s, I_G is linearly proportional to stomatal conductance (Jones, 1999a), as demonstrated under a wide range of conditions (Maes & Steppe, 2012). This index uses the same references as $RWSI_1$ but gives low values in stressed crops and higher values with increasing stomatal conductance (Costa et al., 2013).

$$I_G = \frac{T_{dry} - T_{rosette}}{T_{rosette} - T_{wet}} \quad (3)$$

Three additional RWSIs evaluated on almond orchards (Poirier-Pocovi & Bailey, 2020) were also incorporated and tested in this study. $RWSI_2$ (Equation 4) is similar to $RWSI_1$ but the numerator in the case of $RWSI_2$ is the difference between T_{dry} and $T_{rosette}$:

$$RWSI_2 = \frac{T_{dry} - T_{rosette}}{T_{dry} - T_{wet}} \quad (4)$$

In theory, $T_{rosette}$ is always much higher than T_{wet} except when VPD is close to zero or the rosette is wet (Poirier-Pocovi & Bailey, 2020). Excluding the previously mentioned conditions, it is expected that $RWSI_2$ will (1) show values between zero and one and (2) increase with decreasing $T_{rosette}$ and increasing plant/crop stomatal opening.

It would be more practical if one of the two reference surfaces is not needed for the estimation of a stress index. The wet surface is especially problematic as it needs to be continually rewetted. $RWSI_{dry}$ normalizes $T_{dry} - T_{rosette}$ with T_{dry} (Poirier-Pocovi & Bailey, 2020):

$$RWSI_{dry} = \frac{T_{dry} - T_{rosette}}{T_{dry}} \quad (5)$$

According to the authors, since T_{dry} is expected to be equal or higher than T_{leaf}, the index is, in theory, expected to (1) have values equal (when leaf is not transpiring) or bigger (when leaf is transpiring) than zero and (2) increase with increasing plant/crop stomatal opening (Poirier-Pocovi & Bailey, 2020).

$RWSI_{wet}$ normalizes $T_{rosette} - T_{wet}$ with T_{wet} (Poirier-Pocovi & Bailey, 2020):

$$RWSI_{wet} = \frac{T_{rosette} - T_{wet}}{T_{wet}} \quad (6)$$

According to the authors, since T_{leaf} is expected to be equal or higher than T_{wet}, the index is expected to (1) have values equal or bigger than zero and (2) increase with increasing plant/crop stomatal closure (Poirier-Pocovi & Bailey, 2020).

2.6 | Statistical analysis

Jamovi (Version 1.2; jamovi.org) was used for statistical analysis. One-way analysis of variance (ANOVA) followed by Tukey post hoc test ($p < 0.05$) was employed to test the effect of salinity on soil water potential. Two-way ANOVA, using light environment and salinity as fixed factors, followed by Tukey post hoc test ($p < 0.05$) was employed to test the effect of the two factors on projected leaf area, rosette fresh and dry weight, rosette WC, rosette temperature, rosette transpiration rate, and stress indices among plants treated

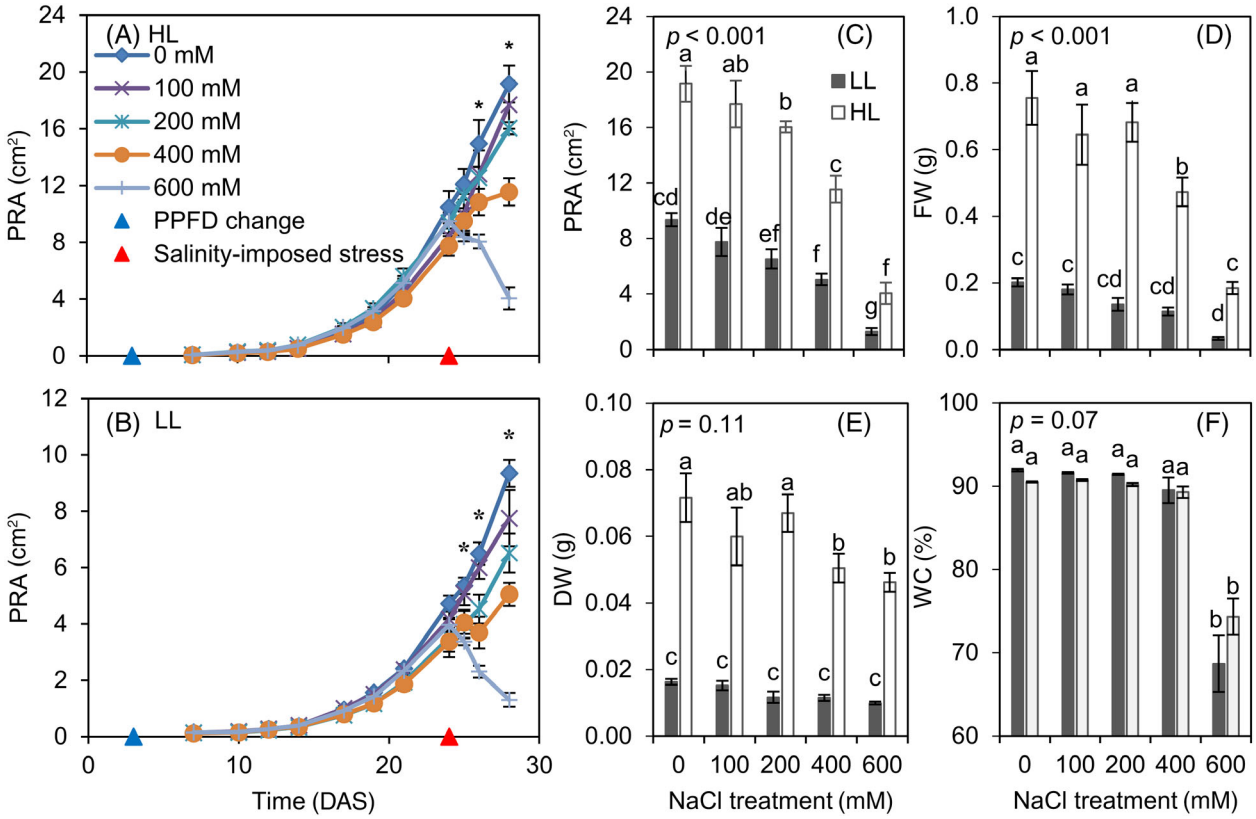

FIGURE 2 (A,B) Projected rosette area (PRA change over time after placing the plants under the two photosynthetic photon flux densities levels (blue triangle) and until 4 days after the salinity-imposed stress (red triangle) at high (HL) (A) and low light (LL) intensity (B). Stars indicate the presence of statistically significant differences between the salinity treatments ($p < 0.05$; $n = 5$). (C–F) The final PRA (C), rosette fresh weight (FW; D), rosette dry weight (DW; E), and rosette water content (WC; F) of *Arabidopsis* plants grown under the high (white bars; HL) and LL intensity (gray bars; LL) treated with different salinity levels. Different letters above the bars indicate significant differences between the means ($p < 0.05$; $n = 5$ measurements, each on an five independent plant) by two-way analysis of variance (Tukey test). Error bars indicate the standard error of the mean. The *p*-value on the top of each bar graph indicates significant interaction between light environment and salinity ($p \leq 0.05$). DAS, days after stratification.

with different salinity levels grown under LL and HL conditions. Multiple regression analysis (MRA) was employed to assess the relation between *E* and each of the indices, also considering light and time of measurement as predictor variables (categorical expressed as dummy variables). Autocorrelation, collinearity, and normality tests were performed during the MRA. Finally, the two-way linear associations (i.e., correlations) between rosette transpiration, rosette temperature, and the different indices used in this study were tested using Pearson correlation coefficient (*r*), and correlation matrices were prepared to summarize and visualize possible associations between the selected variables. The scale used for the interpretation of the size of a correlation coefficient is based on Mukaka (2012).

3 | RESULTS

3.1 | Rosette growth

The PRA showed an exponential increase in time irrespective of the light environment prior to the salinity imposition (Figure 2A,B). PRA increase rate was much higher under HL when compared with LL, resulting in twofold higher final PRA of plants grown under control conditions (0 mM NaCl treatment, $\Psi_{soil} = -0.15$ MPa; Figure 1A) at the end of the experiment (Figure 2C). Statistically significant differences in PRA between the salinity levels were observed a day after salinity imposition for plants grown under LL and the subsequent day for plants grown under HL (Figure 2A,B). More specifically, at LL and HL, plants treated with 600 mM NaCl ($\Psi_{soil} = -0.86$ MPa) exhibited significantly lower PRA than control plants at Days 25 and 26, respectively.

At the end of the experiment, PRA, FW, and DW were lower at LL than HL irrespective of the salinity level (Figure 2C–E), while rosette WC did not show differences between LL and HL (Figure 2F). At HL, plants subjected to ≥200 mM NaCl ($\Psi_{soil} \geq -0.24$ MPa) showed significantly lower PRA and plants subjected to ≥400 mM NaCl ($\Psi_{soil} \geq -0.49$ MPa) showed significantly lower FW compared with the control plants (Figure 2C,D). At LL, plants subjected to ≥200 mM NaCl showed significantly lower PRA and plants subjected to 600 mM NaCl showed significantly lower FW in comparison with control plants (Figure 2C,D). At LL, no significant difference was

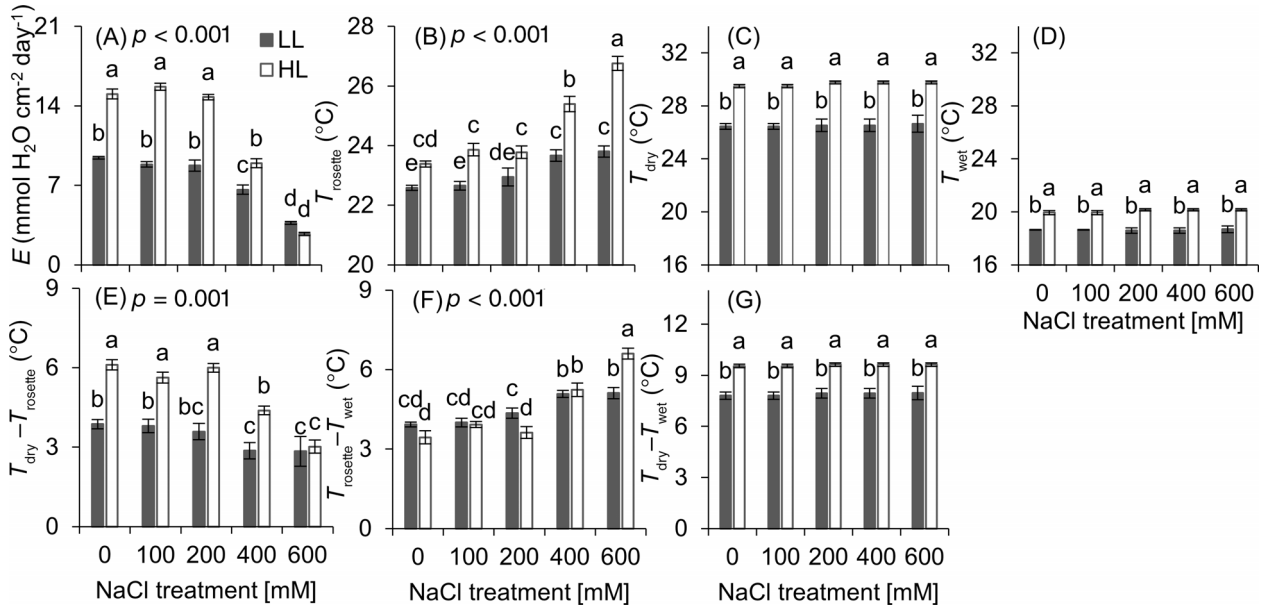

FIGURE 3 (A) Rosette transpiration rate (E), (B) rosette temperature ($T_{rosette}$), (C) dry surface temperature (T_{dry}), (D) wet surface temperature (T_{wet}) measured, (E) $T_{dry} - T_{rosette}$, (F) $T_{rosette} - T_{wet}$, and (G) $T_{dry} - T_{wet}$ calculated at Day 2 for *Arabidopsis* plants grown under the high (HL; white bars) and low light (LL) intensity (gray bars) treated with different salinity levels. Different letters above the bars indicate significant differences between the means ($p < 0.05$; $n = 5$ measurements, each on an five independent plant) by two-way analysis of variance (Tukey test). Error bars indicate the standard error of the mean. The p-value on the top of each bar graph indicates significant interaction between light environment and salinity ($p \leq 0.05$).

observed in DW between salinity treatments, while plants subjected to ≥400 mM NaCl at HL showed significantly lower DW compared with the control plants (Figure 2E). Rosette WC was significantly lower only for plants subjected to 600 mM NaCl at both light environments (Figure 2F). Significant interactions between the light environment and salinity were only observed for PRA ($p < 0.001$) and FW ($p < 0.001$).

3.2 | Rosette transpiration, rosette temperature, and stress indices

Rosette transpiration rate (E) was higher in plants grown in HL than LL under 0 mM NaCl (Figure 3A). This difference diminished with increasing salinity levels and E was eventually comparable between plants under HL at 600 mM NaCl and plants under LL. E significantly decreased in plants under ≥400 mM NaCl when compared to 0 mM NaCl, irrespective of the light environment. No substantial differences were observed between Day 2 (Figure 3) and Day 4 (Figure S3) regarding E, $T_{rosette}$, and the reference temperatures. Small differences, if any, are noted in the text below.

$T_{rosette}$ was higher in plants grown in HL than LL, especially at high salinity levels (Figure 3B). $T_{rosette}$ significantly increased in plants under ≥400 mM NaCl when compared with 0 mM NaCl, irrespective of the light environment.

T_{dry} was higher in HL than LL and no significant differences were observed when the dry surface was imaged together with plants treated with different salinity levels (Figure 3C). T_{wet} was also higher in HL than LL and no significant differences were observed when the wet surface was imaged together with plants treated with different salinity levels (Figure 3D). The difference in T_{dry} between HL and LL was larger when compared with T_{wet} and that resulted in higher $T_{dry} - T_{wet}$ under HL (Figure 3G). T_{dry} was always higher and T_{wet} always lower than $T_{rosette}$.

$T_{dry} - T_{rosette}$ ranged between approximately 2°C and 6°C across salinity levels and light environments (Figure 3E). $T_{dry} - T_{rosette}$ was higher in plants grown in HL than LL under 0 mM NaCl. This difference diminished with increasing salinity levels. $T_{dry} - T_{rosette}$ significantly decreased in plants under ≥400 mM NaCl compared with 0 mM NaCl in HL and LL-Day 4 (Figure S3E). No significant differences were observed across salinity levels in LL-Day 2 (Figure 3E).

$T_{rosette} - T_{wet}$ ranged between approximately 3°C and 7°C across salinity levels and light environments (Figure 3F). $T_{rosette} - T_{wet}$ significantly increased in plants under ≥400 mM NaCl compared with 0 mM NaCl, irrespective of the light environment. Significant interactions between the light environment and salinity were observed for E, $T_{rosette}$, $T_{dry} - T_{rosette}$, and $T_{rosette} - T_{wet}$ ($p \leq 0.001$).

$RWSI_1$ was higher in plants grown in LL than HL under 0 mM NaCl (Figure 4A,B). This difference diminished with increasing salinity levels. $RWSI_1$ significantly increased in plants under ≥400 mM NaCl compared with 0 mM NaCl, irrespective of the light environment. No substantial differences were observed between Day 2 (Figure 4A) and Day 4 (Figure 4B).

I_G and $RWSI_2$ were higher in plants grown in HL than LL under 0 mM NaCl (Figure 4C–F). This difference diminished with increasing salinity levels. $RWSI_2$ and I_G significantly decreased in plants under

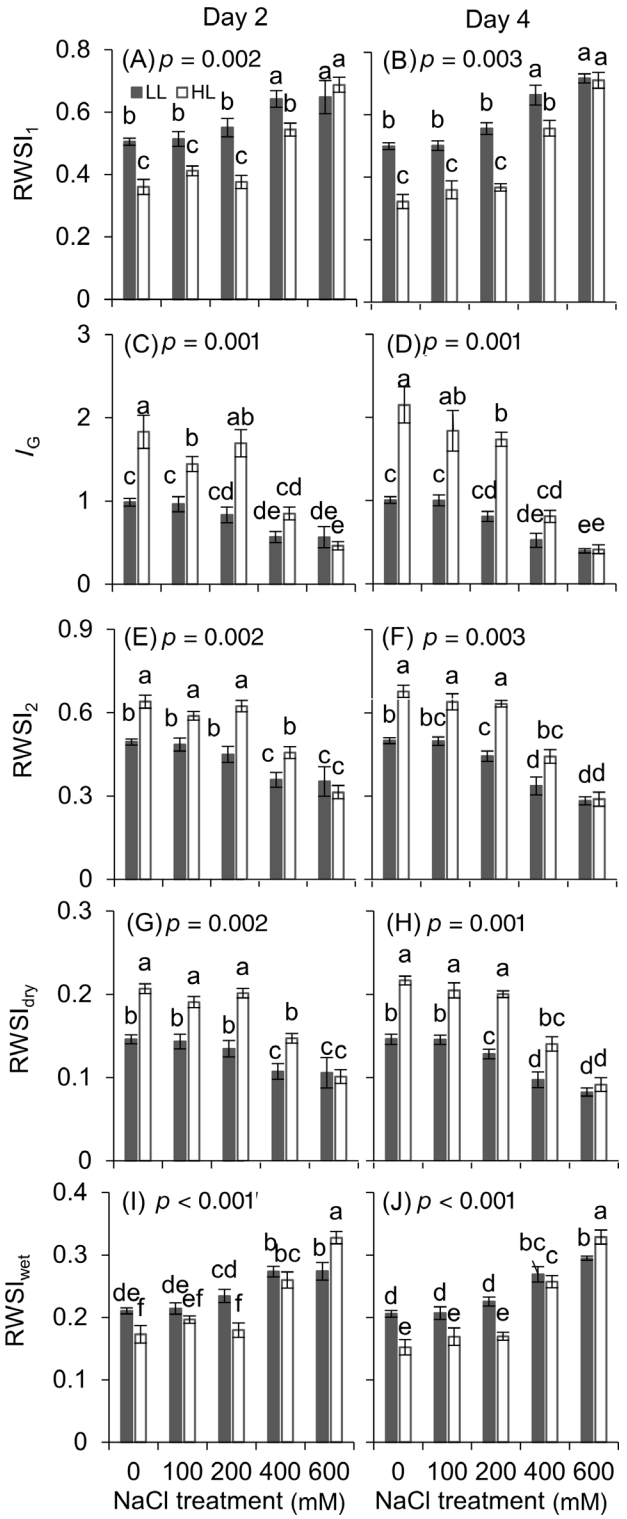

FIGURE 4 $RWSI_1$, I_G, $RWSI_2$, $RWSI_{dry}$, and $RWSI_{wet}$ at Day 2 and Day 4 of *Arabidopsis* plants grown under the high (HL; white bars) and low light (LL) intensity (gray bars) treated with different salinity levels. Different letters above the bars indicate significant differences between the means ($p < 0.05$; $n = 5$ measurements, each on an independent plant) by two-way analysis of variance (Tukey test). Error bars indicate the standard error of the mean (SEM). The *p*-value on the top of each bar graph indicates significant interaction between light environment and salinity ($p \leq 0.05$).

≥400 mM NaCl when compared with 0 mM NaCl, irrespective of the light environment on Day 2. Concerning Day 4, $RWSI_2$ significantly decreased in plants under ≥200 mM NaCl in LL (Figure 4F).

$RWSI_{dry}$ was higher in plants grown in HL than LL under 0 mM NaCl (Figure 4G,H). This difference diminished with increasing salinity levels. $RWSI_{dry}$ significantly decreased in plants under ≥400 mM NaCl in LL-Day 2, and HL-Day 2–4 (Figure 4G,H), and under ≥200 mM NaCl under LL-Day 4 compared with 0 mM NaCl (Figure 4H).

$RWSI_{wet}$ significantly increased in plants under ≥400 mM NaCl compared with 0 mM NaCl, irrespective of the light environment (Figure 4I,J). $RWSI_{wet}$ was higher in plants grown in LL than HL at low salinity levels and the difference was progressively reversed with increasing salinity levels. No substantial differences were observed between Day 2 (Figure 4I) and Day 4 (Figure 4J).

Significant interactions between the light environment and salinity were observed for $RWSI_1$, I_G, $RWSI_2$, $RWSI_{dry}$, and $RWSI_{wet}$ ($p < 0.05$).

3.3 | Relating water stress indices to rosette transpiration rate

MRA was used to assess the relation between *E* and each of the indices also considering the light environment and the day of measurement as predictor variables. No association was observed between the day of measurement and *E* response ($p > 0.05$) irrespective of the index incorporated in the model. MRA after model reduction (i.e., model simplification by eliminating the insignificant terms, i.e., day of measurement) is presented in Table 1. The variation in light environment was significantly associated with variations in *E* ($p < 0.001$) only when $T_{rosette}$, $T_{dry} - T_{rosette}$, $T_{rosette} - T_{wet}$, and $RWSI_{wet}$ were incorporated as predictor variables in the models (Table 1). In these models, based on adjusted R^2, the percentage of variation in the response that was explained by the model was ranging between 0.82 and 0.87 (Table 1). Variations in light environment were positively related to variations in *E* when $T_{rosette}$, $T_{rosette} - T_{wet}$, or $RWSI_{wet}$ were incorporated and negatively when $T_{dry} - T_{rosette}$ was incorporated as predictor variables. The standardized coefficient (β; Navarro & Foxcroft, 2022) enables the comparison of the relative importance of each predicting variable in the regression model. The importance of light as predicting variable was high when combined with $T_{rosette}$ and decreased when reference temperatures were incorporated in different combinations with $T_{rosette}$ (Table 1).

$T_{rosette}$, $T_{dry} - T_{rosette}$, $T_{rosette} - T_{wet}$, and $RWSI_{wet}$ were plotted against *E* individually for LL and HL (Figure 5A–D), indicating the dependence of the relation between these variables and *E* on the light environment. The coefficient of determination (R^2) of these relations suggested a stronger linear relation between *E* and the latter variables at HL (R^2 ranges between 0.88 and 0.89) in comparison with LL (R^2 ranged between 0.43 and 0.64; Figure 5A–D).

Variation in light environment was not significantly associated with variations in *E* when $RWSI_{dry}$, $RWSI_1$, $RWSI_2$, or I_G were incorporated as predictor variables in the models (Table 1). Regression

TABLE 1 Multiple regression analyses per index between rosette transpiration rate and two explanatory variables, the index and light environment.

	Model coefficients						Model fit measures		
Index	**Predictor**	***B***	**SE**	***t***	***β***	***p***	***R***	R^2	Adj. R^2
$T_{rosette}$	Intercept	84.33	3.69	22.80		**<0.001**	0.92	0.85	0.85
	Light	9.68	0.48	20.30	2.17	**<0.001**			
	Index	−3.34	0.16	−20.80	−1.11	**<0.001**			
$T_{dry} - T_{rosette}$	Intercept	−3.17	0.66	−4.83		**<0.001**	0.91	0.82	0.82
	Light	−2.38	0.50	−4.79	−0.53	**<0.001**			
	Index	3.32	0.18	18.70	1.05	**<0.001**			
$T_{rosette} - T_{wet}$	Intercept	23.31	0.74	31.60		**<0.001**	0.93	0.87	0.87
	Light	3.85	0.34	11.20	0.86	**<0.001**			
	Index	−3.53	0.16	−22.30	−0.86	**<0.001**			
$RWSI_{wet}$	Intercept	24.28	0.85	28.68		**<0.001**	0.92	0.85	0.84
	Light	2.41	0.37	6.51	0.54	**<0.001**			
	Index	−69.44	3.40	−20.42	−0.85	**<0.001**			
$RWSI_{dry}$	Intercept	−4.48	0.71	−6.33		**<0.001**	0.91	0.83	0.83
	Light	−0.82	0.45	−1.83	−0.18	0.07			
	Index	97.57	5.13	19.01	0.95	**<0.001**			
$RWSI_1$	Intercept	25.66	0.95	27.04		**<0.001**	0.92	0.84	0.83
	Light	0.31	0.41	0.77	0.07	0.445			
	Index	−31.25	1.60	−19.59	−0.90	**<0.001**			
$RWSI_2$	Intercept	−5.59	0.74	−7.56		**<0.001**	0.92	0.84	0.83
	Light	0.31	0.41	0.77	0.07	0.445			
	Index	31.25	1.60	19.59	0.90	**<0.001**			
I_G	Intercept	2.16	0.47	4.61		**0.005**	0.89	0.79	0.78
	Light	−0.33	0.49	−0.68	−0.07	0.496			
	Index	7.19	0.44	16.43	0.90	**<0.001**			

Note: Significant difference in bold values, $p < 0.05$; light: low and high; B: unstandardized coefficient; SE: standard error; β: standardized coefficient.

analysis after further model reduction (i.e., excluding light environment) revealed the relation between E and $RWSI_1$, $RWSI_2$, $RWSI_{dry}$, or I_G (Figure 5E–H). E was linearly and positively correlated with $RWSI_{dry}$ ($R^2 = 0.82$; Figure 5E), $RWSI_2$ ($R^2 = 0.84$; Figure 5G), I_G ($R^2 = 0.78$; Figure 5H), and negatively correlated with $RWSI_1$ ($R^2 = 0.84$; Figure 5F). However, the relation between E and I_G was eventually better fitted in a polynomial curve mainly due to the wider range of I_G values observed at high compared to low E levels ($R^2 = 0.85$; Figure 5H).

The correlation matrices based on two-way linear associations between all the variables (i.e., indices and E) tested in MRA, separately for each light environment (Figure 6A,B) and overall (Figure 6C), enable further insight. At a first glance, higher correlations were observed between most of the variables tested under HL (Figure 6A) than LL (Figure 6B). Incorporating the data from both light environments resulted in reduction in correlation coefficients, especially when $T_{rosette}$ was related to the rest of the variables including E (Figure 6C). Concerning E, very high correlations ($|r| \geq 0.9$) were observed with $RWSI_{dry}$, $RWSI_1$, and $RWSI_2$ (Figure 6C). At HL, E was very highly correlated ($|r| \geq 0.9$) with all the indices, including $T_{rosette}$, except I_G ($r = 0.89$; Figure 6B). At LL, E was highly correlated ($0.7 < |r| < 0.9$) with all the indices, including $T_{rosette}$, except $T_{dry} - T_{rosette}$ ($r = 0.66$; Figure 6A). Concerning $T_{rosette}$, an overall high correlation ($0.7 \leq |r| \leq 0.9$) was observed with $T_{rosette} - T_{wet}$, while moderate correlation ($0.5 < |r| < 0.7$) was observed with $RWSI_{wet}$, low correlations ($0.3 < |r| < 0.5$) with $RWSI_{dry}$, $RWSI_1$, $RWSI_2$ and I_G, and no correlation with $T_{dry} - T_{rosette}$ (Figure 6C). At HL, $T_{rosette}$ was very highly correlated ($|r| \geq 0.9$) with all the indices (Figure 6B). At LL, $T_{rosette}$ was very highly correlated with $T_{rosette} - T_{wet}$ and highly correlated with all the rest indices, except $T_{dry} - T_{rosette}$ ($r = -0.65$; Figure 6A). Considering the indices other than $T_{rosette}$, they all showed very high or high correlations between them at low (Figure 6A) or high (Figure 6B) or both (Figure 6C) light environments. Overall, the highest correlations were observed for indices that were calculated based on the same temperatures (e.g., $RWSI_1$, $RWSI_2$, and I_G) or indices that share a certain combination of temperatures, for example, $RWSI_{dry}$ and $T_{dry} - T_{rosette}$ (Figure 6C). Interestingly, very high correlations were also observed between $T_{dry} - T_{rosette}$ and the four most prominent indices derived from MRA, $RWSI_1$, $RWSI_2$, $RWSI_{dry}$, and I_G (Figure 6C).

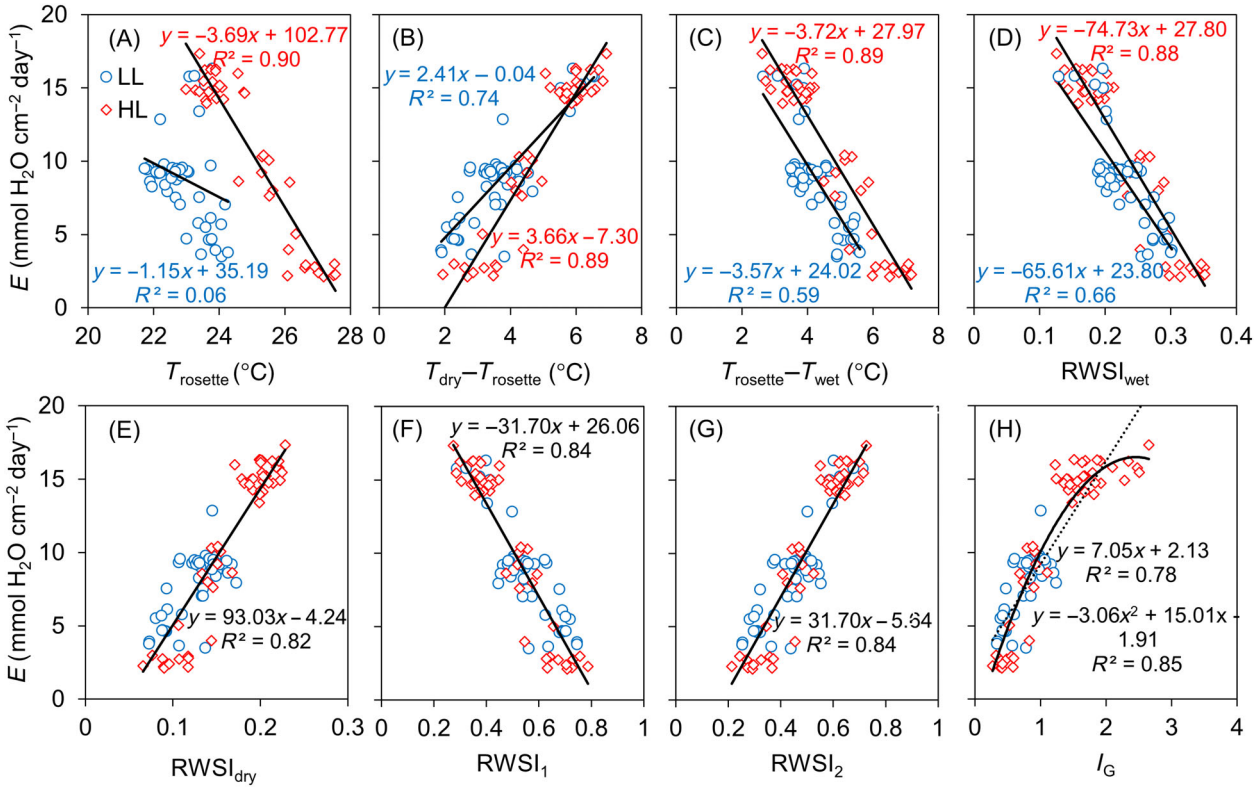

FIGURE 5 The relations between rosette transpiration rate (E) and $T_{rosette}$ (A), $T_{dry} - T_{rosette}$ (B), $T_{rosette} - T_{wet}$ (C), $RWSI_{wet}$ (D), $RWSI_{dry}$ (E), $RWSI_1$ (F), $RWSI_2$ (G), and I_G (H). Circles and rhombus represent plants grown under low light (LL) and high light (HL) intensity, respectively. The dashed line (in H) represents the linear and the solid line represents the polynomial relation between E and I_G.

4 | DISCUSSION

The negative impacts of salinity and water limitation on *A. thaliana* growth are well described in literature using advanced phenotyping tools (Aguirrezabal et al., 2006; Awlia et al., 2016; Clauw et al., 2015; De Diego et al., 2017; Van Der Weele et al., 2000). In this study, salinity negatively affected the PRA and biomass of *A. thaliana* plants irrespective of light intensity. Nevertheless, in comparison with plants grown under HL, plants grown under LL were affected earlier regarding PRA, and light environment significantly influenced the salinity effects on the final biomass and PRA. Despite the differences observed between the two light environments, rosette WC was maintained across the increasing salinity levels and was significantly reduced only when plants were treated with 600 mM NaCl ($\Psi_{soil} = -0.86$ MPa), irrespective of the light intensities, due to the higher reduction of FW than DW. Based on growth traits, it can be indicated that *Arabidopsis* plants in this study were subjected to salinity stress ranging from low to severe, covering in this way a wide range of stress levels.

When facing water limitations, plants respond by closing their stomata to reduce transpiration rates (Figure 3A) and thus maintain their internal water status (Figure 2F). Even though rosette transpiration is considered an essential trait for plant water stress responses, its quantification using typical methodologies (e.g., gravimetric or gas exchange measurements) is quite laborious. $T_{rosette}$ can be used as a good indicator of the variations in E when latent heat loss through transpiration is reduced due to water stress, only under steady aerial conditions (Figures 5A and 6A,B). However, $T_{rosette}$ cannot be safely used as a good indicator of E if another factor shaping leaf heat budget (e.g., radiative heat) is varying and thus influencing $T_{rosette}$ (Figures 5A and 6C). In a natural environment, HL levels are usually accompanied by high thermal radiation levels (i.e., increased radiative heat load) that tend to increase leaf temperatures when other influential factors are maintained constant (Jones, 1992). Similarly, even in more controlled environments, such as the experimental growth room used in this study, specific light sources (e.g., high pressure sodium lamps or fluorescent tubes) irradiate toward the canopy, the resulting heat increased plant temperatures (Janda et al., 2015; Savvides et al., 2013). Consequently, the effects of factors other than transpiration on T_{leaf} must be normalized to properly assess transpiration.

In this study, the use of reference temperatures together with $T_{rosette}$ to normalize for the aerial environment was successful only when used in certain combinations. Firstly, subtracting $T_{rosette}$ from T_{dry} (Figure 5B) or T_{wet} from $T_{rosette}$ (Figure 5C) alone did not normalize the effects of the environment on $T_{rosette}$ (Table 1). The same applied when $T_{rosette} - T_{wet}$ was divided by T_{wet} ($RWSI_{wet}$; Figure 5D). The previously mentioned indicate that reference temperatures in these combinations cannot or cannot fully normalize for the effect of the studied environments on $T_{rosette}$. Accordingly, normalizations with only one of either T_{dry} or T_{wet} were proven insufficient at removing

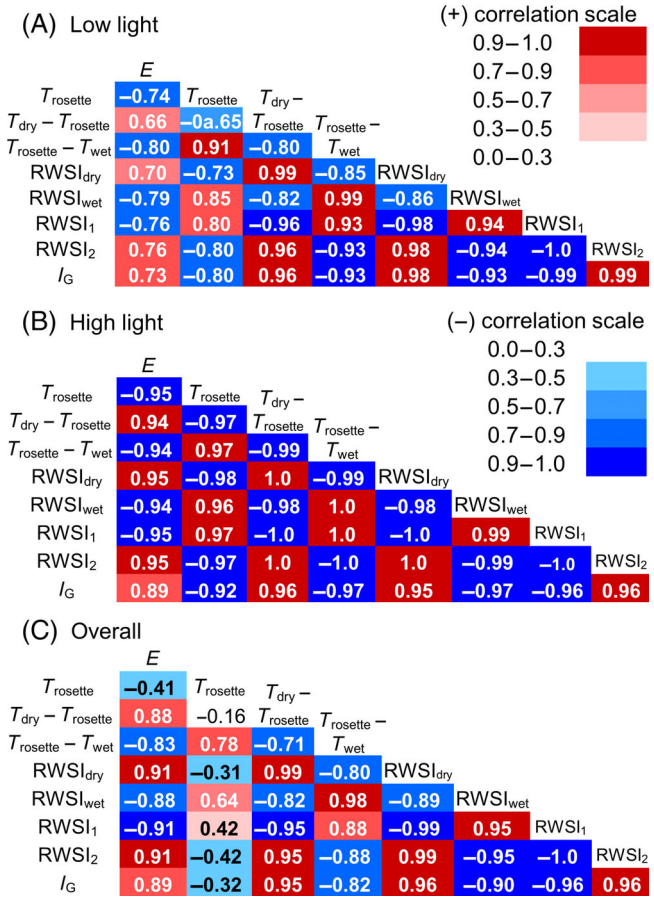

FIGURE 6 Correlation matrices indicating the correlations among rosette transpiration rate (E), $T_{rosette}$, $T_{dry} - T_{rosette}$, $T_{rosette} - T_{wet}$, $RWSI_{dry}$, $RWSI_{wet}$, $RWSI_1$, $RWSI_2$, and I_G at low light (A), high light (B), and overall (C). Bold numbers in cells indicate significant differences at $p < 0.05$. Pearson coefficient (r), the value in each cell for each combination of variables, is a measure of the strength of the linear association and ranges from 0 (negligible association) to 1 (very high association). Negative (blue shades) or positive (red shades) signs indicate whether the linear association between the two variables is either positive (i.e., their values increase or decrease together) or negative (i.e., as the one decreases the other increases and vice versa). The strength of each linear association was characterized as negligible (|0.0| − |0.3|), low (|0.3| − |0.5|), moderate (|0.5| − |0.7|), high (|0.7| − |0.9|), or very high (|0.9| − |1.0|).

the sensitivity of stress indices to factors other-than-stomatal conductance tested in previous studies (Poirier-Pocovi & Bailey, 2020). More specifically, a sensitivity analysis based on almond trees showed that, in sunny conditions, the combination of reference and rosette temperatures used for $RWSI_{wet}$ was sensitive to variations in wind speed, radiation, RH, T_{air}, and stomatal conductance, while the combination used for $RWSI_{dry}$ was sensitive to wind speed, radiation, and stomatal conductance (Poirier-Pocovi & Bailey, 2020). $RWSI_{dry}$ in this study, was well related to E irrespective of the radiation environment ($R^2 = 0.82$; Figure 5E) but not better than $RWSI_1$ ($R^2 = 0.84$; Figure5F) and $RWSI_2$ ($R^2 = 0.84$; Figure5G). In detail, it seems that dividing $T_{dry} - T_{rosette}$ by T_{dry} normalized for other-than-transpiration effects on $T_{rosette}$ to a great extend while dividing by $T_{dry} - T_{wet}$ yielded a better relationship with E.

According to Jones (2004), E is proportional to $T_{dry} - T_{leaf}$ but a constant of proportionality is necessary for any given conditions. It is reasonable to hypothesize that quantifying the temperature of a dry surface, or a non-transpiring surface, with $T_{rosette}$ assists in normalizing for other-than-transpiration effects on $T_{rosette}$. According to Maes and Steppe (2012), $T_{dry} - T_{leaf}$ can be a simplified index that avoids the use of a wet reference surface, mainly since the influence of weather conditions and leaf characteristics on this index is similar to that of I_G. In this study, even though $T_{dry} - T_{rosette}$ was not sufficient to normalize for other-than-transpiration effects on $T_{rosette}$ (Table 1, Figure 5B), it was very highly correlated with all the most prominent indices irrespective the light environment (Figure 6C), a fact that indicates its high importance as a component of an index. Comparing $RWSI_{dry}$ with the other prominent indices, $RWSI_1$, $RWSI_2$, and I_G, it could be speculated that the involvement of T_{wet} in the normalization attempted is minor in comparison with T_{dry} but necessary to achieve better associations with E (Figure 5). However, further study is needed to assess the relative contribution of the dry and wet surface temperatures in E assessment (e.g., Poirier-Pocovi & Bailey, 2020).

$RWSI_1$ was negatively correlated with E, while $RWSI_2$ and I_G, were positively and strongly correlated, irrespective of the radiation environment (Figures 5F–H and 6C). It should be noted here that

$RWSI_1$, $RWSI_2$, and I_G comprised of the same three parameters (i.e., $T_{rosette}$, T_{dry}, and T_{wet}) in different combinations. In fact, $RWSI_1 = 1 - RWSI_2$ and $RWSI_1 = (1 + I_G)^{-1}$. Consequently, when $RWSI_1$ is linearly and negatively related to E, a linear and positive relation would be expected for $RWSI_2$ and a non-linear and positive relation would be expected for I_G. Jones (1992) indicated that the water stress index in the form of $RWSI_1$ (Equation 2) is better related to E than stomatal conductance. Alchanatis et al. (2010), working with cotton plants, showed that, using artificial reference temperatures, CWSI is linearly related to $1 - (E/E_{pot})$, a parameter that actually represents the change in E related to the potential transpiration from a well-watered crop (i.e., $[E_{pot} - E]/E_{pot}$). According to Maes and Steppe (2012), there is no firm theoretical relation between $RWSI_1$ and $1 - (E/E_{pot})$ due to the use of T_{wet} instead of T_{pot} (i.e., the temperature of a crop with potential transpiration), therefore E cannot be precisely estimated using artificial references and the selected water stress index. However, that does not necessarily impact the ability of $RWSI_1$ (or $RWSI_2$) to approximate changes/differences in E, as highlighted in this study (Figure 5F,G). The combination of reference and rosette temperatures used for $RWSI_1$ here (i.e., CWSI) was further related to stomatal resistance (Ben-Gal et al., 2009) and stem water potential in olive trees and cotton plants (Ben-Gal et al., 2009; Cohen et al., 2005) in previous studies.

I_G was linearly related to stomatal conductance in many previous studies tested on different species under a wide range of weather conditions (Jones, 1999a, 1999b, 2002; Maes & Steppe, 2012), while $RWSI_1$ was related to stomatal conductance but not linearly (Jones, 1999a; Maes & Steppe, 2012). It can be therefore suggested that, when relating water stress to E, it is preferable to use $RWSI_1$ or $RWSI_2$ rather than I_G and the inverse when relating water stress to stomatal conductance.

In addition, we here show that under reduced radiation levels, the relation between E and $T_{rosette}$ is much weaker (Figure 5A), supporting the notion that related experimentation or plant phenotyping using thermal indices under low radiation levels may not give clear insights, especially when using instrumentation of low temperature resolution or accuracy (Jones, 2018). Similarly, Poirier-Pocovi and Bailey (2020) indicated that sunny, instead of shaded, conditions may be necessary to capture the effects of water status using thermal imaging because the radiative term in the leaf energy balance amplifies the latent cooling term and thus the sensitivity of leaf temperature to stomatal conductance.

Despite the large difference in PRA and E between the plants growing at different radiation environments and the microclimatic differences between the two light environments, $RWSI_1$ or $RWSI_2$ were closely tracking E differences based on $T_{rosette}$, T_{dry}, and T_{wet} measurements using thermal imaging. This indicates that, among others, the reference surfaces chosen were appropriate for *A. thaliana* under the experiment environments. However, reference surfaces resembling leaf/canopy traits, especially influencing leaf/canopy energy balance, should be preferred (Jones, 2018; Prashar & Jones, 2016).

The stress indices used provide instantaneous measurements. Such instantaneous measurements, despite being taken only during the morning, were well related to the rosette transpiration per day under controlled conditions (Figure 5). Stomatal conductance, even under constant light environments in controlled conditions, may show diurnal patterns (e.g., Boccalandro et al., 2012), and it can thus be assumed that stress indices estimated based on repeated measurements within a day may also follow such patterns. On the one hand, the strong association between daily rosette transpiration and selected stress indices suggests that possible diurnal patterns in stomatal conductance are not as influential for E assessment using instantaneous measurements under the present growth conditions. On the other hand, more measurements within a day (e.g., Agam et al., 2013) may yield better estimations of E and possible diurnal patterns.

Overall, within the microclimatic growth conditions tested in this study for *A. thaliana*, $RWSI_1$ or $RWSI_2$ can be successfully utilized as an index for E. In contrast, the sole use of either of the reference surface temperatures (T_{wet}, T_{dry}) in different combinations studied here can give less accurate results. Regarding the utilization of $RWSI_1$, $RWSI_2$, or I_G as stress indices, it should be noted that E or stomatal conductance may fluctuate with radiation and other non-stress factors. A combination of thermal imaging with other techniques, such as fluorescence or hyperspectral imaging, can give more comprehensive insights into the impact of stress on plant function and growth (Gerhards et al., 2019; Jangra et al., 2021). The artificial reference surfaces used were substantial and easy to obtain and utilize. However, other recently tested artificial reference surfaces may be easier to use or better approximating the surface of a non- and a maximal-transpiring leaf (Jones, 2018; Maes et al., 2016; Vialet-Chabrand & Lawson, 2020). Additionally, the results in this study were obtained under steady-state conditions. A recent study compared stress indices (such as $RWSI_1$ and I_G) with gas exchange parameters and indicated limitations of the stress indices used in a dynamic environment (Vialet-Chabrand & Lawson, 2020). Vialet-Chabrand and Lawson (2020) suggested that these limitations can be overcome using artificial leaf surfaces with known conductance. Lastly, although the experiment was performed under controlled conditions, differences in $T_{rosette}$ were observed between the light treatments under non-limiting-water conditions due to differences in the radiative heat emitted. Consequently, caution should be taken for the co-existence of temperature and light effects on plants during experimentation under controlled conditions.

AUTHOR CONTRIBUTIONS

Andreas M. Savvides designed and performed the experiments and data analysis and wrote the manuscript. Aaron I. Velez-Ramirez performed the image analysis. Vasileios Fotopoulos and Aaron I. Velez-Ramirez read and commented on the manuscript. Andreas M. Savvides, Aaron I. Velez-Ramirez and Vasileios Fotopoulos revised the manuscript.

ACKNOWLEDGMENTS

We are grateful to Dr Chrystalla Antoniou and Mr Jan Pavlou for their assistance during the experiments. The software used for image analysis was acquired thanks to the financial support from Mexican Consejo Nacional de Ciencia y Tecnologia (CONACyT) via grant 294511.

DATA AVAILABILITY STATEMENT

Data sharing is not applicable to this article as all new created data is already contained within this article.

ORCID

Andreas M. Savvides https://orcid.org/0000-0001-7585-3313
Aaron I. Velez-Ramirez https://orcid.org/0000-0002-4603-0489
Vasileios Fotopoulos https://orcid.org/0000-0003-1205-2070

REFERENCES

Agam, N., Cohen, Y., Berni, J.A.J., Alchanatis, V., Kool, D., Dag, A. et al. (2013) An insight to the performance of crop water stress index for olive trees. *Agricultural Water Management*, 118, 79–86.

Aguirrezabal, L., Bouchier-Combaud, S., Radziejwoski, A., Dauzat, M., Cookson, S.J. & Granier, C. (2006) Plasticity to soil water deficit in *Arabidopsis thaliana*: dissection of leaf development into underlying growth dynamic and cellular variables reveals invisible phenotypes. *Plant, Cell & Environment*, 29, 2216–2227.

Alchanatis, V., Cohen, Y., Cohen, S., Moller, M., Sprinstin, M., Meron, M. et al. (2010) Evaluation of different approaches for estimating and mapping crop water status in cotton with thermal imaging. *Precision Agriculture*, 11, 27–41.

Awlia, M., Nigro, A., Fajkus, J., Schmoeckel, S.M., Negrão, S., Santelia, D. et al. (2016) High-throughput non-destructive phenotyping of traits that contribute to salinity tolerance in *Arabidopsis thaliana*. *Frontiers in Plant Science*, 7, 1414.

Bartlett, M.K., Klein, T., Jansen, S., Choat, B. & Sack, L. (2016) The correlations and sequence of plant stomatal, hydraulic, and wilting responses to drought. *Proceedings of the National Academy of Sciences*, 113, 13098–13103.

Ben-Gal, A., Agam, N., Alchanatis, V., Cohen, Y., Yermiyahu, U., Zipori, I. et al. (2009) Evaluating water stress in irrigated olives: correlation of soil water status, tree water status, and thermal imagery. *Irrigation Science*, 27, 367–376.

Boccalandro, H.E., Giordano, C.V., Ploschuk, E.L., Piccoli, P.N., Bottini, R. & Casal, J.J. (2012) Phototropins but not cryptochromes mediate the blue light-specific promotion of stomatal conductance, while both enhance photosynthesis and transpiration under full sunlight. *Plant Physiology*, 158(3), 1475–1484.

Bradski, G. (2000) The OpenCV library. *Dr. Dobb's Journal of Software Tools*, 25, 120–123.

Cabrera, J., Conesa, C.M. & Del Pozo, J.C. (2022) May the dark be with roots: a perspective on how root illumination may bias in vitro research on plant–environment interactions. *New Phytologist*, 233, 1988–1997.

Cirelli, D., Lieffers, V.J. & Tyree, M.T. (2012) Measuring whole-plant transpiration gravimetrically: a scalable automated system built from components. *Trees – Structure and Function*, 26, 1669–1676.

Clauw, P., Coppens, F., De Beuf, K., Dhondt, S., Van Daele, T., Maleux, K. et al. (2015) Leaf responses to mild drought stress in natural variants of *Arabidopsis*. *Plant Physiology*, 167, 800–816.

Cohen, Y., Alchanatis, V., Meron, M., Saranga, Y. & Tsipris, J. (2005) Estimation of leaf water potential by thermal imagery and spatial analysis. *Journal of Experimental Botany*, 56, 1843–1852.

Corwin, D.L. (2021) Climate change impacts on soil salinity in agricultural areas. *European Journal of Soil Science*, 72, 842–862.

Costa, J.M., Grant, O.M. & Chaves, M.M. (2013) Thermography to explore plant-environment interactions. *Journal of Experimental Botany*, 64, 3937–3949.

Daryanto, S., Wang, L. & Jacinthe, P.A. (2017) Global synthesis of drought effects on cereal, legume, tuber and root crops production: a review. *Agricultural Water Management*, 179, 18–33.

De Diego, N., Fürst, T., Humplík, J.F., Ugena, L., Podlešáková, K. & Spíchal, L. (2017) An automated method for high-throughput screening of *Arabidopsis* rosette growth in multi-well plates and its validation in stress conditions. *Frontiers in Plant Science*, 8, 1702.

Filippou, P., Antoniou, C. & Fotopoulos, V. (2011) Effect of drought and rewatering on the cellular status and antioxidant response of *Medicago truncatula* plants. *Plant Signaling & Behavior*, 6, 270–277.

Filippou, P., Zarza, X., Antoniou, C., Obata, T., Villarroel, C.A., Ganopoulos, I. et al. (2021) Systems biology reveals key tissue-specific metabolic and transcriptional signatures involved in the response of *Medicago truncatula* plant genotypes to salt stress. *Computational and Structural Biotechnology Journal*, 19, 2133–2147.

Flexas, J., Bota, J., Loreto, F., Cornic, G. & Sharkey, T.D. (2004) Diffusive and metabolic limitations to photosynthesis under drought and salinity in C3 plants. *Plant Biology*, 6, 269–279.

Gerhards, M., Schlerf, M., Mallick, K. & Udelhoven, T. (2019) Challenges and future perspectives of multi-/hyperspectral thermal infrared remote sensing for crop water-stress detection: a review. *Remote Sensing*, 11, 1240.

González Guzmán, M., Cellini, F., Fotopoulos, V., Balestrini, R. & Arbona, V. (2022) New approaches to improve crop tolerance to biotic and abiotic stresses. *Physiologia Plantarum*, 174, e13547.

Idso, S.B., Jackson, R.D., Pinter, P.J., Reginato, R.J. & Hatfield, J.L. (1981) Normalizing the stress-degree-day parameter for environmental variability. *Agricultural Meteorology*, 24, 45–55.

Jackson, R.D., Idso, S.B., Reginato, R.J. & Pinter, P.J. (1981) Canopy temperature as a crop water stress indicator. *Water Resources Research*, 17, 1133–1138.

Jackson, R.D., Reginato, R.J. & Idso, S.B. (1977) Wheat canopy temperature: a practical tool for evaluating water requirements. *Water Resources Research*, 13, 651–656.

Janda, M., Navrátil, O., Haisel, D., Jindřichová, B., Fousek, J., Burketová, L. et al. (2015) Growth and stress response in *Arabidopsis thaliana*, *Nicotiana benthamiana*, *Glycine max*, *Solanum tuberosum* and *Brassica napus* cultivated under polychromatic LEDs. *Plant Methods*, 11, 1–14.

Jangra, S., Chaudhary, V., Yadav, R.C. & Yadav, N.R. (2021) High-throughput phenotyping: a platform to accelerate crop improvement. *Phenomics*, 1, 31–53.

Jones, H.G. (1992) *Plants and microclimate: a quantitative approach to environmental plant physiology*. Cambridge: Cambridge University Press.

Jones, H.G. (1999a) Use of infrared thermometry for estimation of stomatal conductance as a possible aid to irrigation scheduling. *Agricultural and Forest Meteorology*, 95, 139–149.

Jones, H.G. (1999b) Use of thermography for quantitative studies of spatial and temporal variation of stomatal conductance over leaf surfaces. *Plant, Cell and Environment*, 22, 1043–1055.

Jones, H.G. (2002) Use of infrared thermography for monitoring stomatal closure in the field: application to grapevine. *Journal of Experimental Botany*, 53, 2249–2260.

Jones, H.G. (2004) Application of thermal imaging and infrared sensing in plant physiology and ecophysiology. *Advances in Botanical Research*, 41, 107–163.

Jones, H.G. (2018) Thermal imaging and infrared sensing in plant ecophysiology. In: Sánchez-Moreiras, A.M. & Reigosa M.J. (Eds.) *Advances in Plant Ecophysiology Techniques*. Springer, pp. 135–151.

Jones, H., Serraj, R., Loveys, B., Xiong, L., Wheaton, A. & Price, A. (2009) Thermal infrared imaging of crop canopies for the remote diagnosis and quantification of plant responses to water stress in the field. *Functional Plant Biology*, 36, 978–989.

Klem, K., Mishra, K.B., Novotná, K., Rapantová, B., Hodaňová, P., Mishra, A. et al. (2016) Distinct growth and physiological responses of *Arabidopsis thaliana* natural accessions to drought stress and their detection using spectral reflectance and thermal imaging. *Functional Plant Biology*, 44, 312–323.

Lawson, T. & Vialet-Chabrand, S. (2019) Speedy stomata, photosynthesis, and plant water use efficiency. *New Phytologist*, 221, 93–98.
Maes, W.H., Baert, A., Huete, A.R., Minchin, P.E.H., Snelgar, W.P. & Steppe, K. (2016) A new wet reference target method for continuous infrared thermography of vegetations. *Agricultural and Forest Meteorology*, 226–227, 119–131.
Maes, W.H. & Steppe, K. (2012) Estimating evapotranspiration and drought stress with ground-based thermal remote sensing in agriculture: a review. *Journal of Experimental Botany*, 63, 4671–4712.
McAdam, S.A.M. & Brodribb, T.J. (2012) Stomatal innovation and the rise of seed plants. *Ecology Letters*, 15, 1–8.
McAusland, L., Vialet-Chabrand, S., Matthews, J. & Lawson, T. (2015) Spatial and temporal responses in stomatal behaviour, photosynthesis and implications for water-use efficiency. In: Mancuso, S. & Shabala, S. (Eds.) *Rhythms in plants*. Switzerland: Springer, pp. 97–119.
Merlot, S., Mustilli, A.-C., Genty, B., North, H., Lefebvre, V., Sotta, B. et al. (2002) Use of infrared thermal imaging to isolate *Arabidopsis* mutants defective in stomatal regulation. *The Plant Journal*, 30, 601–609.
Meyerowitz, E. (2001) Prehistory and history of *Arabidopsis* research. *Plant Physiology*, 125, 15–19.
Mukaka, M.M. (2012) A guide to appropriate use of correlation coefficient in medical research. *Malawi Medical Journal*, 24, 69–71.
Mukherjee, S., Mishra, A. & Trenberth, K.E. (2018) Climate change and drought: a perspective on drought indices. *Current Climate Change Reports*, 4(2), 145–163.
Munns, R. (2002) Comparative physiology of salt and water stress. *Plant, Cell and Environment*, 25, 239–250.
Navarro, D. & Foxcroft, D. (2022) Learning statistics with jamovi: a tutorial for psychology students and other beginners (version 0.75). DOI: https://doi.org/10.24384/hgc3-7p15.
Orzechowska, A., Trtílek, M., Tokarz, K. & Rozpądek, P. (2020) A study of light-induced stomatal response in *Arabidopsis* using thermal imaging. *Biochemical and Biophysical Research Communications*, 533, 1129–1134.
Pineda, M., Barón, M. & Pérez-Bueno, M.-L. (2021) Thermal imaging for plant stress detection and phenotyping. *Remote Sensing*, 13(1), 68.
Poirier-Pocovi, M. & Bailey, B.N. (2020) Sensitivity analysis of four crop water stress indices to ambient environmental conditions and stomatal conductance. *Scientia Horticulturae*, 259, 108825.
Prashar, A. & Jones, H.G. (2016) Assessing drought responses using thermal infrared imaging. *Methods in Molecular Biology*, 1398, 209–219.
Rice, S.K., Collins, D. & Anderson, A.M. (2001) Functional significance of variation in bryophyte canopy structure. *American Journal of Botany*, 88, 1568–1576.
Ryan, A.C., Dodd, I.C., Rothwell, S.A., Jones, R., Tardieu, F., Draye, X. et al. (2016) Gravimetric phenotyping of whole plant transpiration responses to atmospheric vapour pressure deficit identifies genotypic variation in water use efficiency. *Plant Science*, 251, 101–109.
Savvides, A., Dieleman, J.A., Van Ieperen, W. & Marcelis, L.F.M. (2016) A unique approach to demonstrating that apical bud temperature specifically determines leaf initiation rate in the dicot *Cucumis sativus*. *Planta*, 243, 1071–1079.
Savvides, A., Fanourakis, D. & Van Ieperen, W. (2012) Co-ordination of hydraulic and stomatal conductances across light qualities in cucumber leaves. *Journal of Experimental Botany*, 63, 1135–1143.
Savvides, A.M. & Fotopoulos, V. (2018) Two inexpensive and non-destructive techniques to correct for smaller-than-gasket leaf area in gas exchange measurements. *Frontiers in Plant Science*, 9, 548.
Savvides, A., Van Ieperen, W., Dieleman, J.A. & Marcelis, L.F.M. (2013) Meristem temperature substantially deviates from air temperature even in moderate environments: is the magnitude of this deviation species-specific? *Plant, Cell and Environment*, 36, 1950–1960.
Schneider, C.A., Rasband, W.S. & Eliceiri, K.W. (2012) NIH image to ImageJ: 25 years of image analysis. *Nature Methods*, 9, 671–675.
Tanner, C.B. (1963) Plant temperatures. *Agronomy Journal*, 55, 210–211.
Van Der Weele, C.M., Spollen, W.G., Sharp, R.E. & Baskin, T.I. (2000) Growth of *Arabidopsis thaliana* seedlings under water deficit studied by control of water potential in nutrient-agar media. *Journal of Experimental Botany*, 51, 1555–1562.
Vialet-Chabrand, S. & Lawson, T. (2020) Thermography methods to assess stomatal behaviour in a dynamic environment. *Journal of Experimental Botany*, 71, 2329–2338.
Wituszynska, W. & Karpiński, S. (2014) Determination of water use efficiency for *Arabidopsis thaliana*. *Bio-Protocol*, 4(3), e1041.
Wituszyńska, W., Ślesak, I., Vanderauwera, S., Szechyńska-Hebda, M., Kornaś, A., Van Der Kelen, K. et al. (2013) Lesion simulating disease, enhanced disease susceptibility, and phytoalexin deficient conditionally regulate cellular signaling homeostasis, photosynthesis, water use efficiency, and seed yield in *Arabidopsis*. *Plant Physiology*, 161, 1795–1805.
Zörb, C., Geilfus, C.-M. & Dietz, K.-J. (2019) Salinity and crop yield. *Plant Biology*, 21, 31–38.

SUPPORTING INFORMATION

Additional supporting information can be found online in the Supporting Information section at the end of this article.

How to cite this article: Savvides, A.M., Velez-Ramirez, A.I. & Fotopoulos, V. (2022) Challenging the water stress index concept: Thermographic assessment of *Arabidopsis* transpiration. *Physiologia Plantarum*, 174(5), e13762. Available from: https://doi.org/10.1111/ppl.13762